# Membrane structure correlates to function of LLP2 on the cytoplasmic tail of HIV-1 gp41 protein

Alexander L. Boscia[1], Kiyotaka Akabori[1], Zachary Benamram[1], Jonathan A. Michel[1], Michael S. Jablin[1], Jonathan D. Steckbeck[2,3], Ronald C. Montelaro[2,3], John F. Nagle[1] and Stephanie Tristram-Nagle[1]

[1]Biological Physics Group, Physics Department, Carnegie Mellon University, Pittsburgh, Pennsylvania, USA. [2]Center for Vaccine Research and [3]Department of Microbiology and Molecular Genetics, University of Pittsburgh School of Medicine, Pittsburgh, Pennsylvania, USA.

**SUPPLEMENTARY INFORMATION**

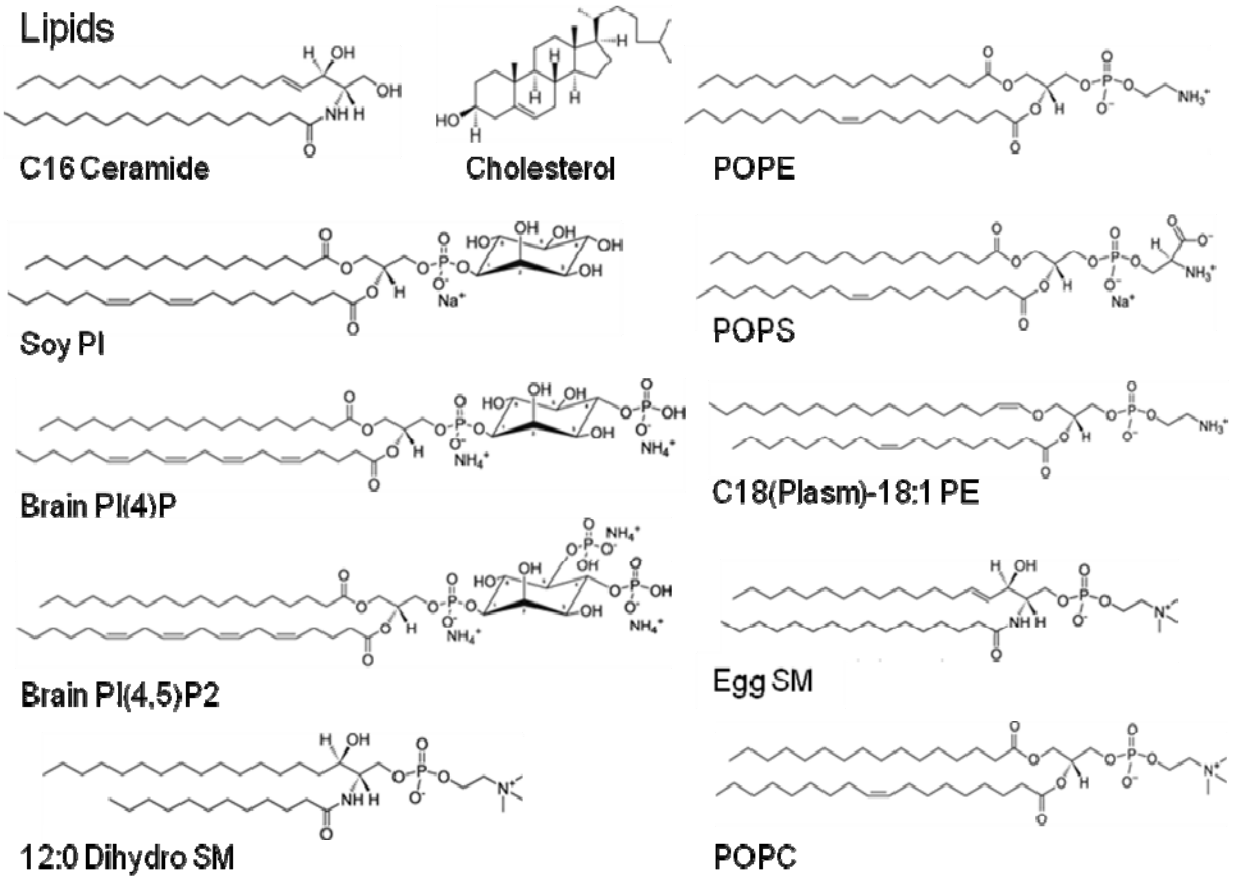


LLP2 variants

| | | |
|---|---|---|
| wild-type (WT) | H2N- | YHRLRDLLLIVTRIVELLGRR-COOH (#764-788) |
| MX2 mutant | H2N- | YHELRDLLLIVTRIVELLGRE-COOH (#764-788) |
| CracWTpal | H2N-C(pal)- | LFLYHRLRDLLLIVTRIVELLGRR-COOH (#761-788) |
| CracWT | H2N-G | LFLYHRLRDLLLIVTRIVELLGRR-COOH (#761-788) |
| CracMX2pal | H2N-C(pal)- | LFLYHELRDLLLIVTRIVELLGRE-COOH (#761-788) |

**Supplementary Figure 1.** Structures of lipid components of membrane mimics (from Avanti Polar Lipids WEBsite) and LLP2 variants. The residues with the cholesterol-binding Crac motif are underlined.

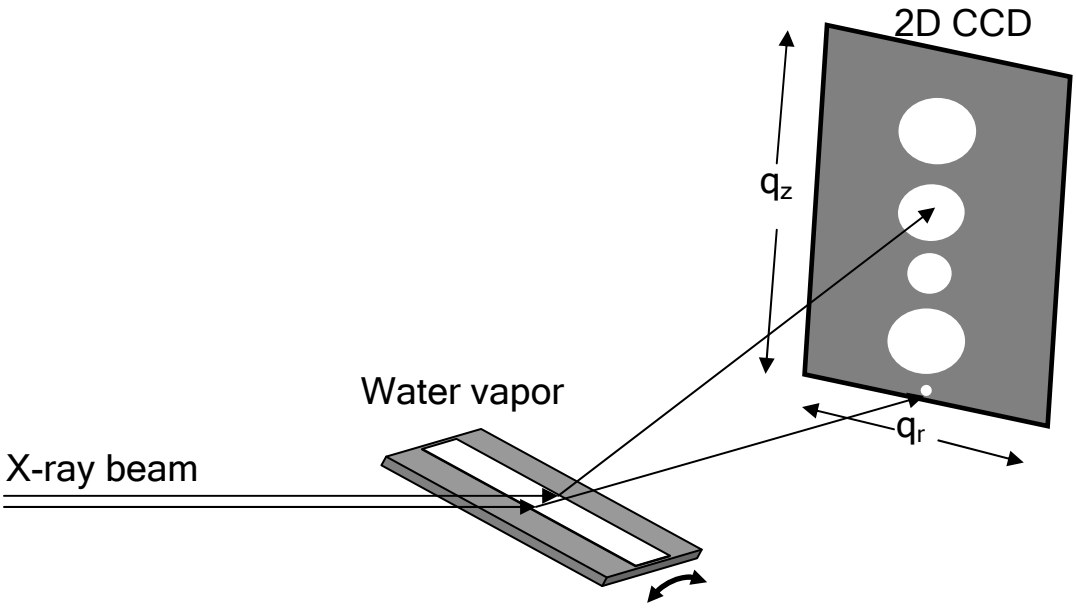


**Supplementary Figure 2.** LAXS geometry. The x-ray beam enters a humidity chamber (not shown) and impinges upon the stacked, membrane mimic sample (shown as white) centered on a silicon wafer which rotates from -1.6 to 7 to -1.6 degrees in one second during the 30-60 second data collection. The scattered intensity is collected on a 2D CCD detector. For WAXS, the data are collected at a positive $0.5^{o}$ fixed angle, and at $-0.5^{o}$ for the background, which are then subtracted from each other. The sample is translated horizontally to avoid radiation damage.

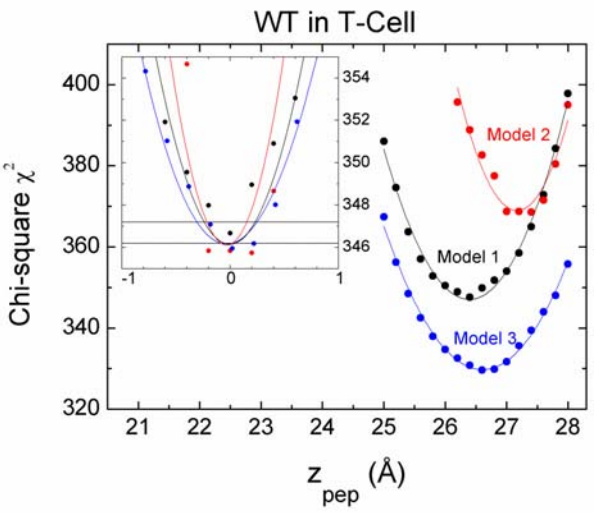


| | $z_{pep}$ | $\delta z_{pep}$ |
|---|---|---|
| **Model 1.** | 26.4 | (-.20 + .16) |
| **Model 2.** | 27.2 | (-.25 + .21) |
| **Model 3.** | 26.6 | (-.30 + .22) |
| **Average** | 26.7 ± 0.34 | |

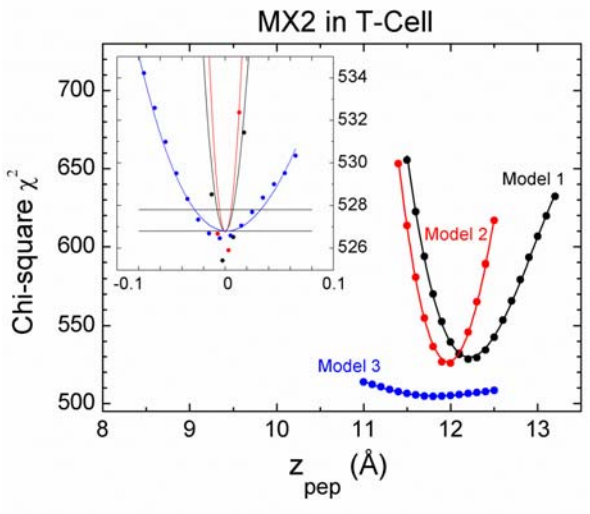


| | $z_{pep}$ | $\delta z_{pep}$ |
|---|---|---|
| **Model 1.** | 12.3 | (-.08 + .08) |
| **Model 2.** | 12.0 | (-.06 + .06) |
| **Model 3.** | 11.8 | (-.26 + .35) |
| **Average** | 12.0 ± 0.17 | |

**Supplementary Figure 3.** Estimating the uncertainties $\delta z_{pep}$ in the positions $z_{pep}$ of the WT and MX2 peptides in the T-cell membrane mimic (40:1). The symbols show $\chi^2$ as a function of $z_{pep}$ obtained by constraining $z_{pep}$ while allowing the other model parameters to fit using the SDP procedure. The solid lines are parabolic or cubic fits to $\chi^2(z_{pep})$. The three models considered were similar SDP models, but there were differences among the constraints. Differences compared to those listed in Materials and Methods were: WT in T-cell mimic Model 1, peptide width free; Model 2, peptide width fixed to 2.8, phosphate headgroup width fixed to 2.0; Model 3, peptide width free, headgroup widths free, DH1 constraint loosened to t=0.1 from 0.05. MX2 in T-cell mimic Model 1, peptide width free; Model 2, peptide width free, r (ratio of terminal methyl to methylene volumes) free, r12 (ratio of peptide to methylene volumes) free; Model 3, peptide width free, r free, r12 free, DH1 constraint loosened to t=0.1 from 0.05. The independently estimated errors $\delta z_{pep}$ for each model (shown in parentheses above) were obtained in a standard way by incrementing the chi-square value from its minimum, adding 1 and reading the peptide position where the fitted curve intersected the straight line at +1 (shown in insets). These errors were generally smaller than the error obtained from the average best positions for the three models. We suggest that $\delta z_{pep} = \pm 0.5$ Å is a conservative estimate.

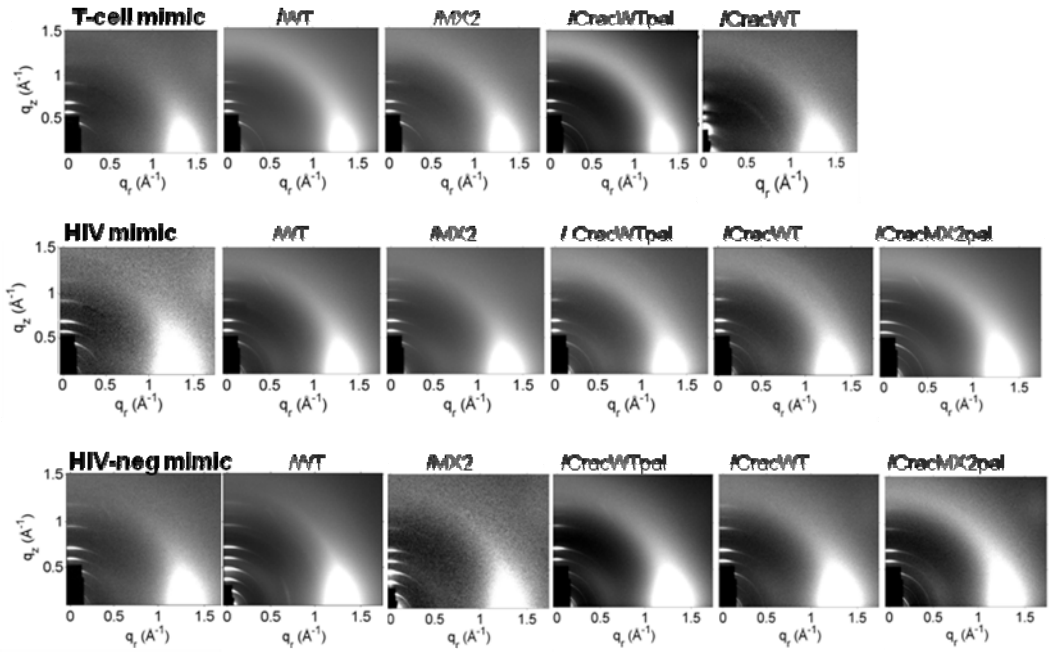


**Supplementary Figure 4.** WAXS from T-cell membrane mimic samples (top row), HIV membrane mimic samples (middle row) and HIV-neg membrane mimic samples (bottom row) all at a lipid:peptide ratio of 20:1. The white ellipse at $q_r \approx 1.4$ Å$^{-1}$ is the hallmark of the liquid-ordered phase (in all samples). $S_{xray}$ was calculated following the procedure of Ref. (14). Mosaic spread α decreases the apparent value of $S_{xray}$. We have calibrated this decrease by smearing ideal data with a mosaic function and subtracting the $S_{xray}$ obtained from the smeared data from the known $S_{xray}$ for the unsmeared data with α=0. Mosaic spread α was quantified using the 5$^{th}$ low-angle lamellar order that appears above the beam stop in the WAXS data (see **Figure 4** and **Supplementary Fig. 4**). This was done by fitting the integrated intensity data of the 5$^{th}$ lamellar order along constant q to obtain a Lorentzian width $\omega_L$, and then applying the following equation:

$$\omega_L^2 = \alpha^2 + 4(0.5^o - \theta_B)^2$$

where $\theta_B$ is half the scattering angle of the 5$^{th}$ order peak and 0.5$^o$ is the incident angle of the beam.

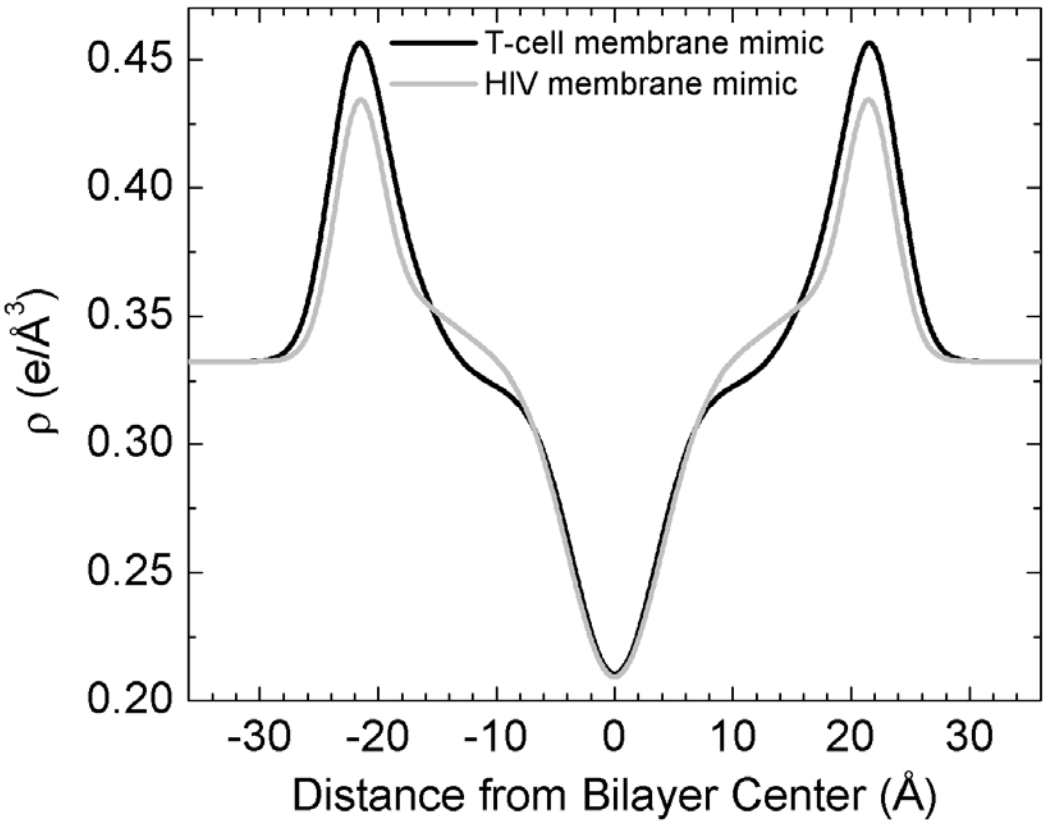


**Supplementary Figure 5.** Total electron density profiles of T-cell and HIV membrane mimics. The higher electron density near 11 Å in the HIV membrane mimic is due to its higher cholesterol content (45% compared to 30% in the T-cell mimic). The lower electron density in the HIV headgroup is due to a larger area/unit cell in the HIV membrane mimic. These profiles result from structural modeling using the SDP program as described in Materials and Methods.

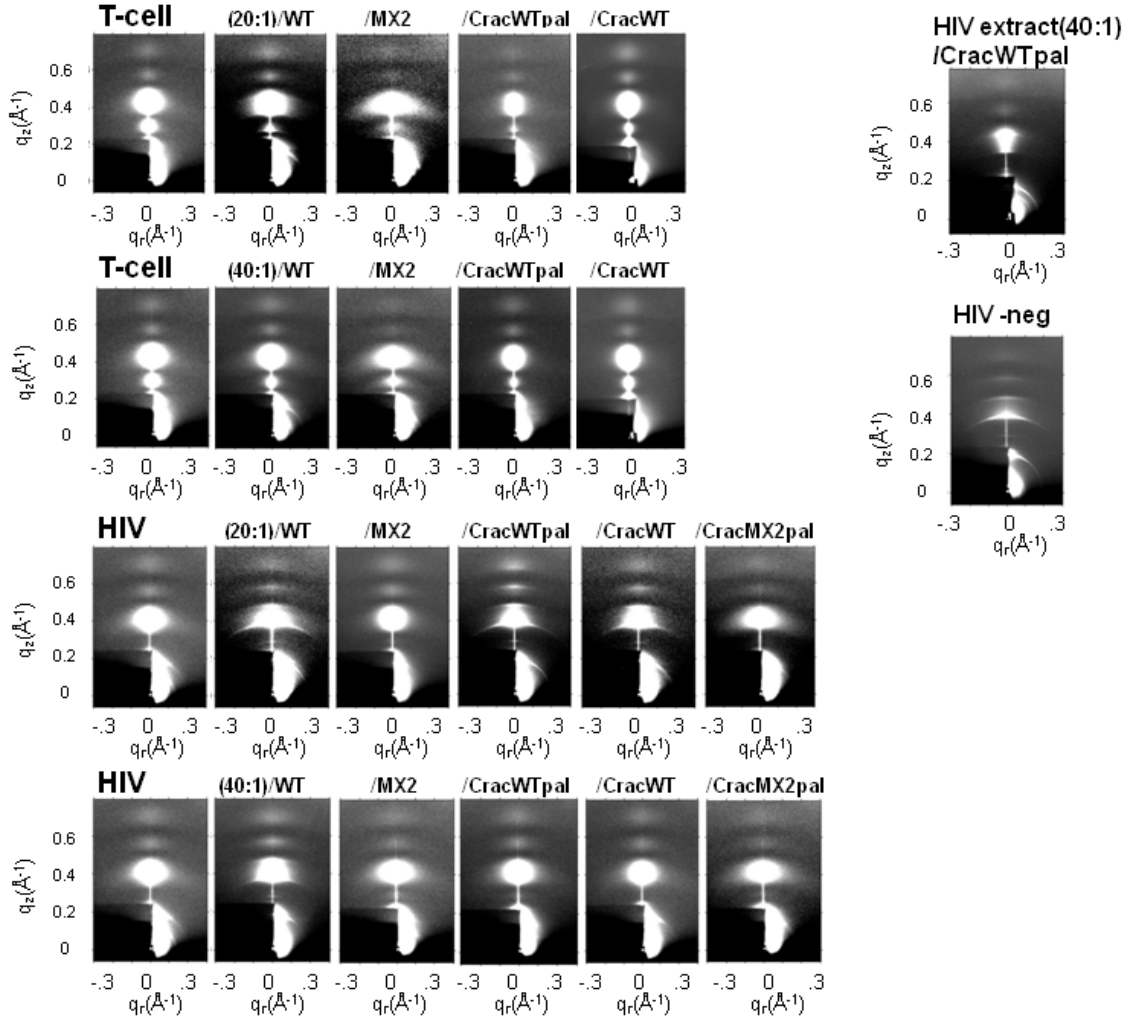


**Supplementary Figure 6.** LAXS from membrane mimics with and without peptides: Tcell mimic with LLP2 peptide variants at 20:1 (first row) and 40:1 (second row) lipid:peptide mole ratios, and HIV mimic with 20:1 (third row) and 40:1 (fourth row). Like the HIV mimic samples, the HIVextract(40:1)/CracWTpal (upper right) also has the second diffuse lobe missing. This HIV extract(40:1)/CracWTpal sample is the best oriented of the HIV extracted lipid samples; due to poor orientation and low signal-to-noise ratios in the other HIV extracted lipid samples, a precise structural analysis was not possible, even though $K_C$ values were able to be obtained (see Table 3 in main paper.) Also shown is HIV-neg membrane mimic (on right). This HIV-neg membrane mimic pattern was not altered by the addition of peptides or by increasing the hydration time. Due to insufficient diffuse data in the HIV-neg membrane mimic samples, a precise structural analysis was not possible, even though $K_C$ values were able to be obtained (see Table 3 in main paper.)

The laterally elongated shape of diffuse lobes for both T-cell and HIV mimic/peptide samples in **Supplementary Fig. 6** is due to a slightly larger mosaic spread, or misalignment, of these samples and does not affect structure. LAXS results from HIV-chol mimic samples are not shown, since there was a phase coexistence of gel and fluid phases (see Fig. 4.d), and our liquid crystal fitting analysis requires a single phase and single D-spacing. LAXS results from all of the HIV–neg membrane mimic samples are also not shown, since there was insufficient diffuse data for structure determination (see one example in **Supplementary Fig. 6**, on upper right).

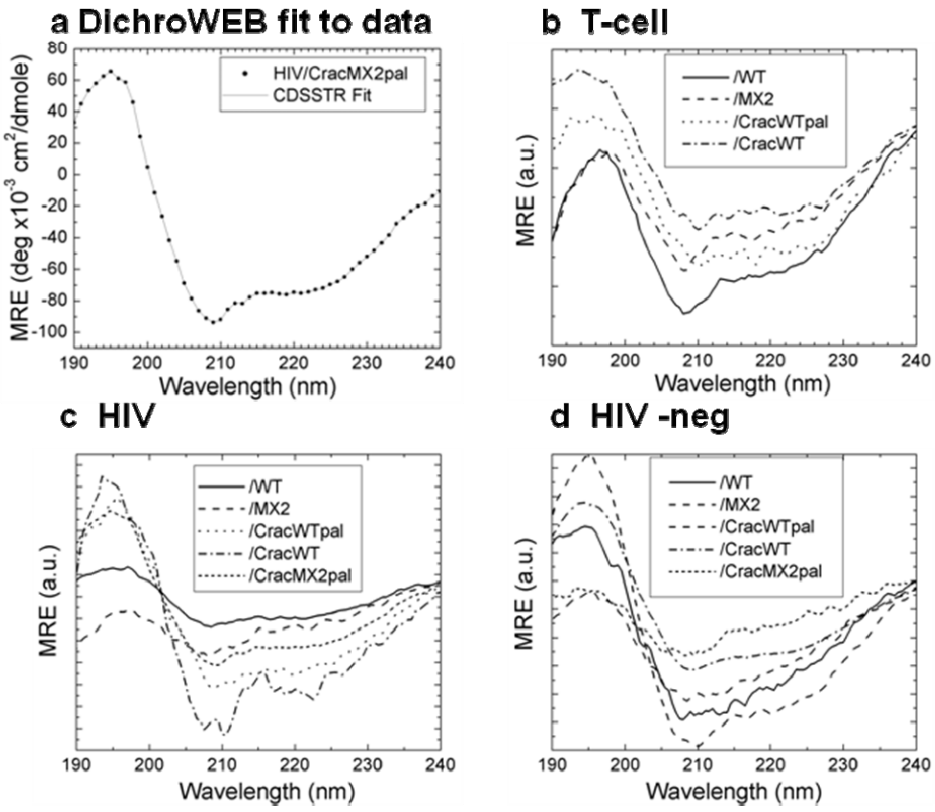


**Supplementary Figure 7.** CD spectra of LLP2 variants in membrane mimics. (**a**) Data for HIV/CracMX2pal and fit to data using the CDSSTR function in the DichroWEB on-line program (see Materials and Methods), (**b**) T-cell membrane mimic samples, (**c**) HIV membrane mimic samples, and (**d**) HIV-neg membrane mimic samples. Spectra are from either the vertical or inverted cuvette position. Cuvette background data were subtracted from these spectra. Traces are scaled vertically to separate the data for visual comparison.

**Supplementary Table 1.** CD results for 20:1 lipid/peptide samples. The unoriented 0.1 μm thick samples were hydrated through the vapor as described in Methods. The CDSSTR fitting function of DichroWEB was used to analyze the CD spectra using basis set #4.

| Sample (20:1) | Helix | β-Strand | Random |
|---|---|---|---|
| **Tcell mimic/** | | | |
| /WT | 55 ± 5 | 24 ± 5 | 21 ± 1 |
| /MX2 | 53 ± 2 | 29 ± 2 | 18 ± 1 |
| /CracWTpal | 65 ± 2 | 23 ± 3 | 12 ± 1 |
| /CracWT | 59 ± 3 | 24 ± 2 | 16 ± 2 |
| **HIV mimic/** | | | |
| /WT | 62 ± 6 | 21 ± 7 | 16 ± 2 |
| /MX2 | 59 ± 3 | 23 ± 2 | 20± 3 |
| /CracWTpal | 65 ± 4 | 19 ± 1 | 16 ± 3 |
| /CracWT | 67 ± 2 | 17 ± 1 | 15 ± 1 |
| /CracMX2pal | 72 ± 3 | 16 ± 2 | 11 ± 2 |
| **HIV –neg mimic/** | | | |
| /WT | 70 ± 2 | 13 ± 3 | 20 ± 2 |
| /MX2 | 62 ± 3 | 18 ± 3 | 20 ± 1 |
| /CracWTpal | 70 ± 3 | 19 ± 2 | 10 ± 3 |
| /CracWT | 69 ± 3 | 19 ± 3 | 13 ± 3 |
| /CracMX2pal | 66 ± 5 | 18 ± 3 | 17 ± 3 |

| Sample | α-Helix (%) | β-Strand (%) | Random (%) |
|---|---|---|---|
| WT | 10 ± 3 | 56 ± 5 | 33 ± 5 |
| MX2 | 13 ± 5 | 59 ± 12 | 29 ± 10 |
| CracWTpal | 6 ± 2 | 58 ± 5 | 34 ± 5 |
| CracWT | 28 ± 3 | 42 ± 4 | 29 ± 4 |

**Supplementary Table 2.** Summary of CD fitting results using CDSSTR function in DichroWEB of LLP2 variants in water (0.008 mg/ml). All LLP2 peptides are primarily β-strand in aqueous solution, with random coil as the second highest component. The α-helical content increases to become the dominant motif when the LLP2 peptides associate with membranes (see **Supplementary Fig. 7** and **Supplementary Table 1**). Similar results were obtained with the CONTINLL fitting algorithm.

We have emphasized in the text that weak binding of LLP2 to the HIV mimic would reduce the net membrane charge, thereby reducing the total repulsive interaction that then tips the balance of intermembrane forces from unbinding to binding. Such a reduction of net bilayer charge would not occur if LLP2 were completely dissociated from the HIV mimic. Here we consider a variant within this latter hypothesis that the LLP2 is completely dissociated and not weakly bound. This variant recognizes that LLP2 and its associated counterions act as a salt between the bilayers and this would also reduce the electrostatic repulsive interaction through Debye screening, without reducing the net bilayer charge. If this way of reducing the electrostatic repulsion were most important, then the bilayer D spacing should become finite whether positively charged WT is added or whether negatively charged MX2 is added. In contradiction, the D spacing was unbound when MX2 was added, whereas it became finite when WT was added, thereby supporting our interpretation that LLP2 is weakly bound to the HIV membrane mimic.